Titanium dioxide-based *Q*-switched dual wavelength in the 1 micron region

H. Ahmad[1,*], M. A. M. Salim[1], Z. A. Ali[1], M. F. Ismail[1], K. Thambiratnam[1], A. A. Latif[2], N. Nayan[3], and S. W. Harun[1]

[1]*Photonics Research Centre (PRC), University of Malaya, Kuala Lumpur 50603, Malaysia*
[2]*Department of Physics, University Putra Malaysia, Serdang 43400, Malaysia*
[3]*Faculty of Electrical and Electronic Engineering, Universiti Tun Hussein Onn Malaysia, Johor Baru 86400, Malaysia*
**Corresponding author: harith@um.edu.my*

Received June 11, 2016; accepted July 8, 2016; posted online July 25, 2016

In this work a passively *Q*-switched dual-wavelength ytterbium-doped fiber laser using a titanium dioxide-based saturable absorber is proposed and proven. The system also utilizes a side-polished fiber in a ring cavity configuration to obtain the desired pulse train. A stable dual-wavelength pulse output is obtained at 1034.7 and 1039.0 nm, with a maximum pulse energy of 2.0 nJ, and a shortest pulse width of 3.2 μs. The generated pulse train is stable, and has a pulse repetition rate from 31.2 to 64.5 kHz.

OCIS codes: 060.3510, 140.3510, 140.3540, 140.3615.
doi: 10.3788/COL201614.091403.

Saturable absorbers (SAs) have recently become the emphasis of substantial research efforts due to the crucial role that they play in the generation of pulse laser outputs from passive systems. SAs are highly sought after for these uses due to their significant saturable absorption rates, high compatibility characteristics, and ultrafast recovery times. Typically, most SAs in use today are based upon single wall carbon nanotubes (SWCNTs) or graphene, as these SAs can be easily integrated into a multitude of all-fiber cavity configurations, particularly in ytterbium-, erbium-[1–3], and thulium-doped[4] fiber lasers, and are capable of operating seamlessly across the three main communications regions of the C-, L-, and S-bands[5–7]. These lasers are able to generate steady pulse trains in a compact, cost-effective, and rugged platform, thus making them highly desirable for real-world uses.

In this aspect, the development of a dual- or multi-wavelength pulse laser for multiple uses, such as communications and sensing, is of particular interest. Passively *Q*-switched dual-wavelength fiber lasers have already been realized using SWCNT[1,8] and graphene[9,10]-based SAs, and this has spurred further research efforts to seek out new materials that could possess better electrical and optical characteristics to be used as SAs. As a result of these efforts, various materials that have now been identified for their potential to be fabricated as SAs. These include compounds from the topological insulator (TI) family comprised of bismuth selenide[11–13] and tellurite selenide[14–16] and transition metal dichalcogenides (TMDs) including molybdenum disulfide (MoS_2)[17,18], molybdenum diselenide ($MoSe_2$)[19], tungsten disulfide (WS_2)[20,21], and tungsten diselenide (WSe_2)[22]. The generation of passively mode-locked output MoS_2 nanoplatelets was first demonstrated in a ytterbium-doped fiber laser (YDFL) with a stable pulse centered at 1054.3 nm[23], and also with a microfiber evanescent field to generate high power and stable dissipative solitons at 1042.6 nm[24]. Other exotic materials have also been identified for their potential for use as SAs, such as black phosphorous (BP)[25–27]. These new materials have allowed new passively *Q*-switched and fiber lasers to be designed, particularly those that can generate dual- or multi-wavelength pulse trains and operate beyond conventional wavelength regimes, such as in the 1 micron region *Q*- using a Bi_2Se_3-based SA[28]. Furthermore, the use of these SAs prevents radical changes to the cavity length, and thus prevents the disruption of the delicate balance of losses in a laser cavity. This is particularly important for the exploitation of nonlinear effects in a laser cavity to generate a dual- or multiwavelength output, as demonstrated in systems using Brillouin or Raman scattering[29,30].

In this aspect, titanium dioxide (TiO_2), a semiconductor belonging to the transition metal oxides (TMO) family, has shown a significant potential for use as an SA, especially in the development of dual-wavelength pulsed outputs. TiO_2 is commonly used in the manufacture of ointments, pigment in paints, and even toothpaste[31], yet possesses optical and electrical characteristics that make it highly desirable as an SA. Femtosecond time-resolved pump-probing indicating a recovery time of about 1.5 ps at room temperature[32], and open-aperture Z-scanning performed on anatase and rutile TiO_2 indicates that anatase TiO_2 exhibits a significant nonlinear optical response as well as possessing saturable absorption characteristics[33]. Despite having a bandgap of ~3.2 eV, or ~387.0 nm, TiO_2-based SAs are found to be able to operate at the visible[34] and infrared[35] spectra as well, thus increasing the potential of the TiO_2-based SA.

When compared to most other SA-based materials, TiO_2 has an advantage of a higher modulation depth of about 40.0%[36] and can be easily fabricated as an SA. Graphene, the typical choice for SAs, suffers from a

number of limitations, including a zero-bandgap that delimits the material's on-off ratio[37]. In the case of MoS_2, its limitation as an SA arises from its operational range, which is restricted to the primarily visible range[23,38], while TI-based SAs allow for efficient operation at the longer wavelength regions of above 1600 nm[14], but not at the shorter wavelength regions. BP has also been applied as an SA; its low modulation depth is only 7.8%, but there has been great interest for exploring BPs as an SA[27].

In this work, a dual-wavelength fiber laser with a passively Q-switched output utilizing a thin film TiO_2-based SA is put forward and demonstrated. The system is capable of generating a pulsed dual-wavelength output, with wavelengths centered at 1034.7 and 1039.0 nm at a channel spacing of approximately 4.3 nm. The system has been demonstrated for operation in the 1.0 μm region using a novel SA using a thin film TMO.

The TiO_2 nanostructures used to fabricate the thin film SA were obtained from Sigma Aldrich (Malaysia) Sdn. Bhd. and used without any further purification. Figure 1(a) shows the TiO_2 nanostructures under field emission scanning electron microscopy (FESEM) imaging, which are between 20.0–50.0 nm in size. UV–Vis spectrum analysis of the sample, given in Fig. 1(b), shows that the TiO_2 nanostructures have a strong absorption band at approximately 354.0 nm. The linear absorption intensity of TiO_2 film, given in Fig 1(c), confirms that the TiO_2-based SA will be able to absorb wavelengths in this operating region and, finally, Fig. 1(d) shows the TiO_2 x–ray diffraction (XRD) diagram, which is obtained directly from the manufacturer and reproduced here without modification.

As the TiO_2 nanostructures used in this work were of the anatase group, the performance of TiO_2 as an SA was tested by embedding it into an agar-based thin film polymer. The thin film was developed by heating 1.0 g of agar in a 50.0 mL of deionized water for 15 min at 300.0°C before the addition of 0.05 g of TiO_2 to the thin film to form the SA. The mixture was continuously stirred before being poured into a 25.0 mL mold and then left to dry at 27.0°C for 3 days. The resulting thin film, as shown in the inset of Fig. 1(a) with the embedded TiO_2 nanostructures, forms the SA and has a measured thickness of 0.15 ± 0.01 mm. Finally, the SA is sandwiched in between two fiber ferrules to allow it to be easily incorporated into a fiber laser circuit.

Figure 2(a) gives the experimental configuration used to measure the fabricated TiO_2 SA's saturable absorption behavior. The setup uses a mode-locked erbium-doped fiber laser (EDFL), combined with a carbon nanotube (CNT)-based SA to generate femtosecond pulses to serve as the seed pulse. The EDFL is observed to have a Q-switching pump power threshold of 29.0 mW, and the pulse train generated has a frequency of 27.6 MHz with a 0.51 ps pulse width. The resulting signal is then amplified using a low dispersion Keopsys erbium-doped fiber amplifier (EDFA) to boost the signal's peak power so that it is enough to fully saturate the TiO_2 sample. The mode-locked pulse shape can change its profile in response to its input current, thus it is also necessary to reshape the pulse by tuning the amplifier current. The use of the EDFA allows for a high average output power of 20.0 mW to be obtained. The circuit is completed using two optical power meters (OPMs), a 3 dB optical coupler (OC), and a variable optical attenuator (VOA), as given in Fig. 2(a). The VOA is used to adjust the launch signal power, which is then equally divided in two by a 3 dB OC, with 50% of the output being directed toward the first OPM, designated OPM 1. The remaining signal portion travels through the TiO_2-based SA, and the output is then directed to the second OPM, designated OPM 2.

The resulting characteristic of the TiO_2-based SA is shown in Fig. 2(b), and is obtained using the formula

$$\alpha = \Delta\alpha/(1 + I/I_s) + \alpha_{ns} \quad (1)$$

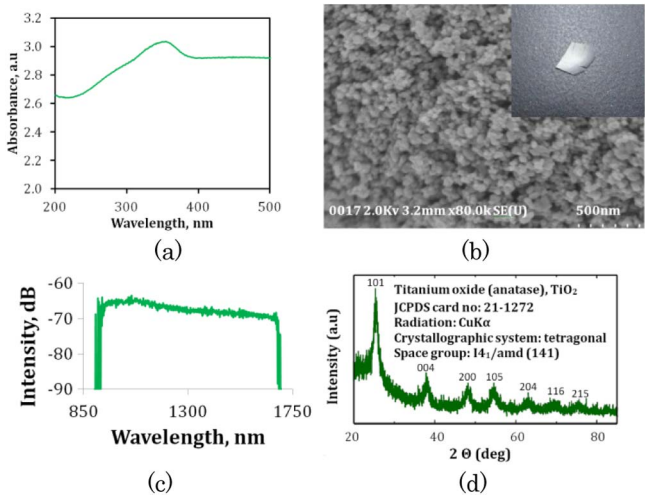

Fig. 1. (a) FESEM image, (b) UV-Vis absorbance, (c) linear absorption, and (d) XRD pattern of TiO_2.

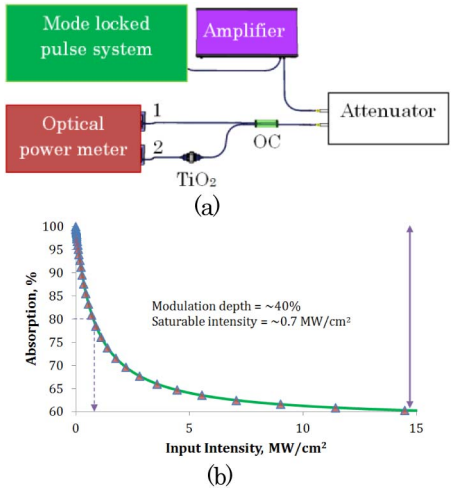

Fig. 2. Configuration for measuring (a) the nonlinear absorption of TiO_2 and (b) the saturable absorption distinctive of the TiO_2 SA.

where is the absorption, I is the intensity, I_s is the saturation intensity, and $\Delta\alpha$ and α_{ns} are the modulation depth and non-saturable losses respectively. The modulation depth as well as the saturable intensity were measured to be approximately 40.0% and 0.7 MW/cm^2, respectively. In this matter, the modulation depth is higher as compared to that obtained using other SAs such as 17.6% for graphene[39], 27.0% for MoS_2[40], 4.7% for $MoSe_2$[19], 3.1% for WS_2[21], 3.02% for WSe_2[22], and 19.5% for BP[25].

The design of the proposed Q-switched dual-wavelength YDFL is presented in Fig. 3. The fiber laser configuration is comprised of a 70 cm DF1100 Fibercore highly-doped 70 cm long ytterbium-doped fiber (YDF), which has a peak absorption of 1300 dB/m at 977 nm. The YDF is pumped by an Oclaro Model LC96A74 P-20 R laser diode (LD) with a center wavelength at 974.0 nm. The pump LD is connected to the laser cavity via the 980 nm port of a 980/1060 nm wavelength division multiplexer (WDM), while the WDM's common port is fusion-spliced to the YDF.

The unconnected end of the YDF is then spliced to an isolator to avoid backward reflection in laser system, and is then connected to a side-polished fiber, which is the primary mechanism for generating the desired dual-wavelength signal[41]. The output from the side-polished fiber is connected to the TiO_2-based SA, which now allows the output to be pulsed. The SA's output is connected to a 90:10 optical circulator, designated OC1 in Fig. 3, with the 90% port being spliced to the 1060 nm port of the WDM, thereby completing the optical cavity. The tapped output from OC1, which is obtained from the 10% port, is now channeled into a 50:50 optical circulator, designated OC2 in Fig. 3. One signal portion is directed to a YOKOGAWA AQ6373 optical spectrum analyzer (OSA), with an operating resolution of 0.02 nm, and serves to provide the optical spectrum of the output. The other signal portion, obtained via the second output port of OC2, is used to analyze the characteristics of the output pulse train, and is connected to a THORLABS InGaAs fiber optic photodetector D400FC which is in turn connected to YOKOGAWA DLM2054 digital oscilloscope. This particular setup is also interchangeable with a THORLABS PM100USB OPM and an Anritsu MS2683A radio frequency spectrum analyzer (RFSA) capable of operating between 9.0 kHz and 7.8 GHz, for further analysis. All the components utilized in the setup are polarization insensitive, thus eliminating the need for a polarization controller in the cavity.

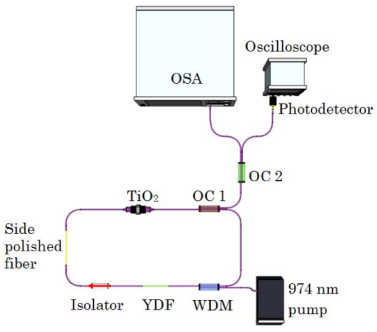

Fig. 3. Experimental setup of TiO_2-based SA in 1 μm region.

Q-switching operation in the laser circuit self starts at an LD power of 143.9 mW, with an initial repetition rate of 31.2 kHz, as shown in Fig. 4(a). As the LD output power is gradually raised to 231.6 mW, a stable pulse at a 62.4 kHz is obtained via an oscilloscope trace, is shown in Fig. 4(b). The repetition rate is reliant linearly on the pump power, a typical behavior of a Q-switched pulse and thus providing validation that the pulses obtained are indeed Q-switched. In the same manner, the pulse width decreases as the pump power increases due to the gain compression[42], again in accordance with the expected behavior of a Q-switched pulse.

Figure 5(a) provides the spectrum of the dual-wavelength output signal. It can be seen that the two pulses are centered at 1034.7 and 1039.0 nm at an LD pump power of 188.0 mW, with the two peaks having output powers of −18.8 and −18.6 dBm, respectively. The conforming Q-switched pulse train is shown in Fig. 5(b), which has a pulse width of 23.0 μs.

The full width at half-maximum (FWHM) of the output pulses is measured to be 3.7 μs, as shown in Fig. 5(c). Figure 5(d) shows the pulse train in the frequency domain as recorded using the RFSA. The trace shows a frequency of 43.5 kHz and has a peak-to-pedestal ratio of 53.0 dB (from the inset) demonstrating stable Q-switched pulse generation.

The repetition rates as well as the corresponding pulse widths in relation to the pump power are shown in Fig. 6(a). As the LD pump power is increased from 143.9 to 239.7 mW, the repetition rate increases as well

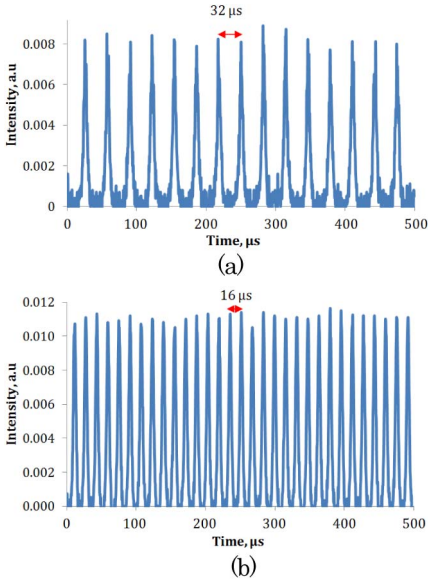

Fig. 4. Changes in pulse duration at (a) 143.90 and (b) 231.60 mW with a frequency of 31.2 and 62.4 kHz, respectively.

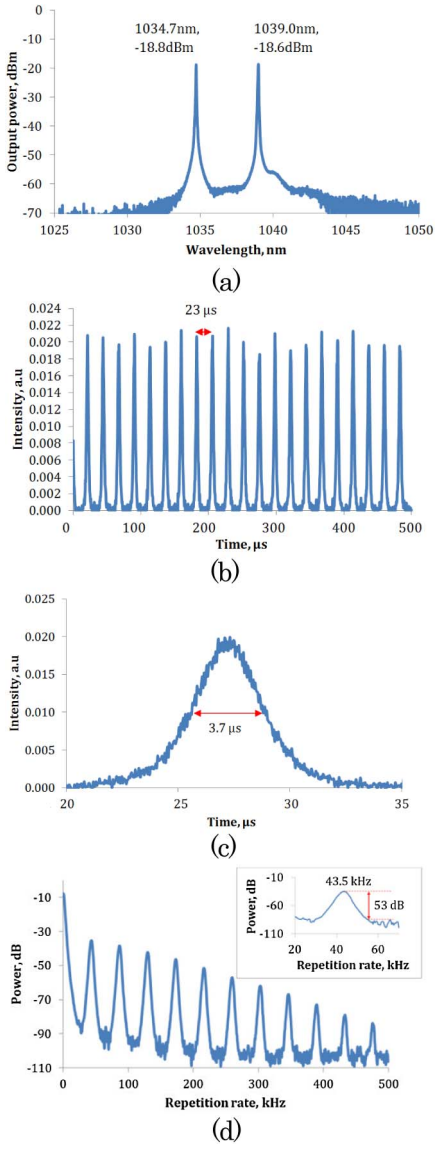

Fig. 5. Distinctive properties of Q-switching: (a) optical domain, (b) pulse duration, (c) pulse width, and (d) frequency domain at a pump LD power of 188.0 mW.

from 31.2 to 64.5 kHz. The pulse width in contrast decreases from 5.6 to 3.2 μs, both of which are typical behaviors of Q-switched pulses. Optimizing the parameters of the proposed setup can narrow the pulse width further, particularly by shortening the optical cavity and optimizing the modulation depth of the TiO_2-based SA[43]. The single-pulse energy and calculated corresponding average output power are also measured, as given in Fig. 6(b).

The pulse energy and the average output power increase linearly with the pump power; the highest average output power was 0.13 mW and the highest pulse energy was 2.0 nJ at a maximum pump power of 239.7 mW. Moreover, higher pulse energies can also be acquired by employing higher-gain fibers, such as a double-clad fibers, as well as by improving the quality of the TiO_2 thin film SA and optimizing the cavity configuration[44]. In addition

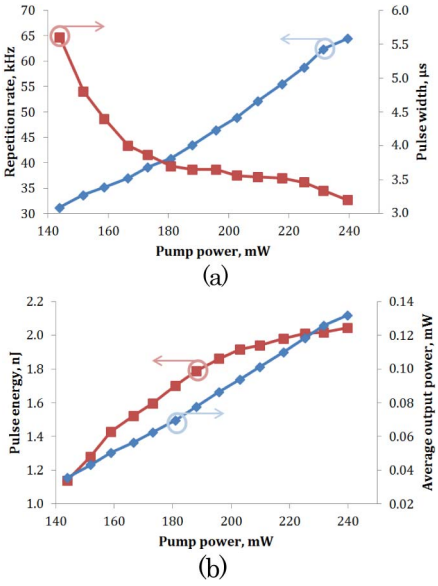

Fig. 6. Correlation between (a) the repetition rate and pulse width and (b) the pulse energy and the average output power corresponding to the pump power.

to that, observation of the output of the laser shows no significant fluctuations, even after 1 h of operation, thus confirming the long-term stability of the system. This also indicates that the SA has not yet suffered any damage, and therefore the damage threshold of the SA is higher than the output of the laser. The proposed system would have multiple uses in the development of cost-effective, compact, and robust fiber-based lasers.

In this work, a passively Q-switched YDFL utilizing a TiO_2-based SA is proposed and demonstrated. A stable Q-switched pulse train with two peak wavelengths centered at 1034.7 and 1039.0 nm is achieved. The pulses have maximum pulse energies of 2.0 nJ and pulse frequencies between 31.2 to 64.5 kHz. The results indicate that TiO_2 is a candidate with a significant potential for producing a Q-switched output in the 1.0 μm region, and can be used to fabricate a simple, low-cost pulsed dual-wavelength fiber laser capable of operating in room conditions.

We would like to thank the University of Malaya for the research funding under LRGS (2015) NGOD/UM/KPT, RU007/2015, and GA010-2014 (Professor Ulung).

References

1. L. Liu, Z. Zheng, X. Zhao, S. Sun, Y. Bian, Y. Su, J. Liu, and J. Zhu, Opt. Commun. **294**, 267 (2013).
2. C. Anyi, N. Ali, A. Rahman, S. Harun, and H. Arof, Ukrainian J. Phys. Opt. **14**, 212 (2013).
3. D.-P. Zhou, L. Wei, B. Dong, and W.-K. Liu, IEEE Photon. Technol. Lett. **22**, 9 (2010).
4. H. Ma, Y. Wang, W. Zhou, J. Long, D. Shen, and Y. Wang, Laser Phys. **23**, 035109 (2013).
5. S. Harun, F. Abd Rahman, K. Dimyati, and H. Ahmad, Laser Phys. Lett. **3**, 536 (2006).
6. S. W. Harun, N. K. Saat, and H. Ahmad, IEICE Electron. Exp. **2**, 182 (2005).

7. M. Mahdi, F. M. Adikan, P. Poopalan, S. Selvakennedy, W. Chan, and H. Ahmad, Opt. Commun. **176**, 125 (2000).
8. T. Feng, K. Yang, S. Zhao, J. Zhao, W. Qiao, T. Li, L. Zheng, J. Xu, Q. Wang, and X. Xu, IEEE Photon. Technol. Lett. **27**, 7 (2015).
9. Z. T. Wang, Y. Chen, C. J. Zhao, H. Zhang, and S. C. Wen, IEEE Photon. J. **4**, 869 (2012).
10. Z. Luo, M. Zhou, J. Weng, G. Huang, H. Xu, C. Ye, and Z. Cai, Opt. Lett. **35**, 3709 (2010).
11. Z. Yu, Y. Song, J. Tian, Z. Dou, H. Guoyu, K. Li, H. Li, and X. Zhang, Opt. Express **22**, 11508 (2014).
12. Z. Q. Luo, Y. Z. Huang, J. Weng, H. H. Cheng, Z. Q. Lin, B. Xu, Z. P. Cai, and H. Y. Xu, Opt. Express **21**, 29516 (2013).
13. H. Ahmad, M. Salim, S. R. Azzuhri, M. Soltanian, and S. Harun, Laser Phys. **25**, 065102 (2015).
14. T. Pinghua, Z. Xiaoqi, Z. Chujun, W. Yong, Z. Han, S. Deyuan, W. Shuangchun, T. Dingyuan, and F. Dianyuan, IEEE Photon. J. **5**, 1500707 (2013).
15. Y. Chen, C. Zhao, S. Chen, J. Du, P. Tang, G. Jiang, H. Zhang, S. Wen, and D. Tang, IEEE J. Sel. Top. Quantum Electron. **20**, 315 (2014).
16. J. Lee, J. Koo, C. Chi, and J. H. Lee, J. Opt. **16**, 085203 (2014).
17. Z. Luo, Y. Huang, M. Zhong, Y. Li, J. Wu, B. Xu, H. Xu, Z. Cai, J. Peng, and J. Weng, J. Lightwave Technol. **32**, 4679 (2014).
18. R. I. Woodward, E. J. Kelleher, R. C. Howe, G. Hu, F. Torrisi, T. Hasan, S. V. Popov, and J. R. Taylor, Opt. Express **22**, 31113 (2014).
19. R. Woodward, R. Howe, T. Runcorn, G. Hu, F. Torrisi, E. Kelleher, and T. Hasan, "Wideband saturable absorption in few-layer molybdenum diselenide (MoSe2) for *Q*-switching Yb-, Er-and Tm-doped fiber lasers," arXiv:1503.08003 (2015).
20. S. H. Kassani, R. Khazaeizhad, H. Jeong, T. Nazari, D.-I. Yeom, and K. Oh, Opt. Mater. Express **5**, 373 (2015).
21. M. Zhang, G. Hu, R. Howe, L. Chen, Z. Zheng, and T. Hasan, "Yb-and Er-doped fiber laser *Q*-switched with an optically uniform, broadband WS2 saturable absorber," arXiv:1507.03188 (2015).
22. B. Chen, X. Zhang, K. Wu, H. Wang, J. Wang, and J. Chen, Opt. Express **23**, 26723 (2015).
23. H. Zhang, S. Lu, J. Zheng, J. Du, S. Wen, D. Tang, and K. P. Loh, Opt. Express **22**, 7249 (2014).
24. J. Du, Q. Wang, G. Jiang, C. Xu, C. Zhao, Y. Xiang, Y. Chen, S. Wen, and H. Zhang, Sci. Rep. **4**, 6346 (2014).
25. T. Jiang, K. Yin, X. Zheng, H. Yu, and X.-A. Cheng, "Black phosphorus as a new broadband saturable absorber for infrared passively *Q*-switched fiber lasers," arXiv:1504.07341 (2015).
26. Y. Chen, G. Jiang, S. Chen, Z. Guo, X. Yu, C. Zhao, H. Zhang, Q. Bao, S. Wen, and D. Tang, Opt. Express **23**, 12823 (2015).
27. L. Kong, Z. Qin, G. Xie, Z. Guo, H. Zhang, P. Yuan, and L. Qian, "Multilayer black phosphorus as broadband saturable absorber for pulsed lasers from 1 to 2.7 um wavelength," arXiv:1508.04510 (2015).
28. H. Ahmad, M. Salim, M. Soltanian, S. R. Azzuhri, and S. Harun, J. Mod. Opt. **62**, 1550 (2015).
29. S. W. Harun, X. Cheng, N. Saat, and H. Ahmad, Electron. Lett. **41**, 174 (2005).
30. S. Harun, M. Shirazi, and H. Ahmad, Laser Phys. Lett. **4**, 678 (2007).
31. J. H. Braun, A. Baidins, and R. E. Marganski, Prog. Org. Coat. **20**, 105 (1992).
32. H. Elim, W. Ji, A. Yuwono, J. Xue, and J. Wang, "Ultrafast optical nonlinearity in PMMA-TiO2 nanocomposites," arXiv:cond-mat/0301153 (2003).
33. K. Iliopoulos, G. Kalogerakis, D. Vernardou, N. Katsarakis, E. Koudoumas, and S. Couris, Thin Solid Films **518**, 1174 (2009).
34. V. N. Kuznetsov and N. Serpone, J. Phys. Chem. B **110**, 25203 (2006).
35. J. T. Luxon and R. Summitt, J. Chem. Phys. **50**, 1366 (1969).
36. H. Ahmad, S. Reduan, Z. Ali, M. A. Ismail, N. Ruslan, C. Lee, R. Puteh, and S. W. Harun, IEEE Photon. J. **8**, 1500107 (2016).
37. S. Lu, L. Miao, Z. Guo, X. Qi, C. Zhao, H. Zhang, S. Wen, D. Tang, and D. Fan, Opt. Express **23**, 11183 (2015).
38. Q. H. Wang, K. Kalantar-Zadeh, A. Kis, J. N. Coleman, and M. S. Strano, Nat. Nanotechnol. **7**, 699 (2012).
39. R. Mary, G. Brown, S. J. Beecher, F. Torrisi, S. Milana, D. Popa, T. Hasan, Z. Sun, E. Lidorikis, and S. Ohara, Opt. Express **21**, 7943 (2013).
40. S. Wang, H. Yu, H. Zhang, A. Wang, M. Zhao, Y. Chen, L. Mei, and J. Wang, Adv. Mater. **26**, 3538 (2014).
41. S. X. Zhang, C. Y. Liu, and H. A. Ye, Appl. Mech. Mater. **602–605**, 2740 (2014).
42. R. Herda, S. Kivistö, and O. G. Okhotnikov, Opt. Lett. **33**, 1011 (2008).
43. C. Zhao, Y. Zou, Y. Chen, Z. Wang, S. Lu, H. Zhang, S. Wen, and D. Tang, Opt. Express **20**, 27888 (2012).
44. A. Martinez, K. Fuse, B. Xu, and S. Yamashita, Opt. Express **18**, 23054 (2010).